Reassessment of the extent of seismic and aseismic slip on the Alaska-Aleutian Megathrust

G13AP00026 to University of Alaska Fairbanks
Period Covered: May 15, 2013 to May 14, 2015 (including no-cost extension)

Jeff Freymueller, Geophysical Institute, University of Alaska Fairbanks, 2156 Koyukuk Drive, Fairbanks, AK 99709

Abstract

In this project, we developed deformation models for two segments of the Alaska-Aleutian megathrust, the Alaska Peninsula segment (1938 earthquake rupture zone), and the Fox Islands segment (the eastern part of the 1957 rupture zone). We focused on the coseismic deformation, mainly constrained by tsunami modeling, and its comparison to the interseismic deformation constrained by present-day GPS data. Our primary goal was to assess the seismic potential of these segments of the megathrust, and determine whether the rupture patterns of past events were consistent with what we infer today from interseismic deformation.

We simulated tsunami propagation for several scenario slip distributions for the 1938 earthquake along the Alaska Peninsula, and compared these to the observed records at Unalaska/Dutch Harbor and Sitka. The Unalaska record is sensitive mainly to the along-strike location of slip, and is fit best by slip that is concentrated in the eastern part of the 1938 rupture zone. The Sitka record is sensitive to the depth of slip but not the location, and is fit best by slip at shallow to intermediate depths. The rupture models that best predict the 1938 tsunami are very consistent with the present day slip deficit inferred from GPS.

We reassessed the slip distribution of the 1957 great Andreanof Islands earthquake in the eastern part of the aftershock zone. Eyewitness reports, historical tide gauge data, and geological evidence for 9–23 m tsunami runups all imply substantial seafloor deformation offshore Unalaska Island during this earthquake, in conflict with the most recently accepted slip models. We simulated the tsunami dynamics for a suite of deformation models that vary in the depth and amount of megathrust slip. Tsunami simulations show that a shallow (5–15 km deep) rupture with ~20 m of slip most closely reproduces the 1957 Dutch Harbor marigram and >18 m runup at Sedanka Island marked by stranded drift logs. Models that place slip deeper than 20 km predict waves that arrive before the 1957 tsunami registered on Dutch Harbor's tide gauge. The coseismic rupture pattern of mainly shallow locking near the trench is consistent with the lack of a clear interseismic deformation signal observed in the present-day GPS data from the region.

Introduction

The seismic and tsunamigenic potential of subduction zones varies from subduction zone to subduction zone, and from segment to segment within a given subduction zone. The potential for future earthquakes can be assessed if we know

the distribution of *slip deficit*, where the slip deficit is the difference between the plate motion rate (and thus long-term slip rate) and the short-term slip rate of aseismic creep. To a simple first-order approximation, slip that does not occur steadily by aseismic creep or as part of transient slow slip events is likely to occur at a later time as coseismic slip in an earthquake (e.g., Savage, 1983; Freymueller et al., 2008; Freymueller, 2011). Measurements of interseismic deformation using GPS, InSAR, and/or other geodetic measurements are the best way to estimate the slip deficit distribution at subduction zones, and this is a critical input for assessments of seismic hazard and tsunami potential.

In this project, we developed deformation models for two segments of the Alaska-Aleutian megathrust, the Alaska Peninsula segment (1938 earthquake rupture zone), and the Fox Islands segment (the eastern part of the 1957 rupture zone). We developed software tools to discretize the Slab 1.0 plate interface model (Hayes et al., 2012), and to compute coseismic and interseismic deformation from slip distributions parameterized on this geometry. We searched for digital copies of the marigrams from the 1938 and 1957 earthquakes, which turned out to be much harder than expected as the original records had in some cases been lost at the National Geophysical Data Center. We conducted a sensitivity study of the slip distribution of the 1938 earthquake, and a detailed modeling study that was able to reconcile the tsunami observations from the 1957 earthquake in the Fox Islands. The latter work, published in Geophysical Research Letters, showed that slip in this easternmost segment of the rupture was much higher than inferred by the slip model of Johnson et al. (1994), and mainly involved slip at relatively shallow depth close to the trench. The coseismic rupture pattern of mainly shallow locking near the trench is consistent with the lack of a clear interseismic deformation signal observed in the present-day GPS data from the region.

This project also included some early work by graduate student Shanshan Li, which ultimately contributed to a paper finally published in 2018 on the modeling of interseismic deformation along the Alaska Peninsula. That work, which was mainly completed after the end of this project, will be briefly summarized here.

1. Sensitivity study for the slip distribution of the 1938 rupture

The 1938 tsunami was recorded on tide gauges in Alaska, North America, Hawaii and Japan (Johnson and Satake, 1994). To compare numerical modeling results with observations, we used records from Unalaska and Sitka, which were the closest tide stations to the 1938 tsunami source area. We used the Sitka record published by Johnson and Satake (1994), and the Unalaska record published by Lander (1996).

To simulate ruptures on the Aleutian megathrust we employed a model of the Alaska–Aleutian plate interface between the subducting and overriding plates. The plate interface model by Hayes et al. (2012) was discretized into a number of rectangles ranging from 3 to 6 km in the along-strike direction of the plate interface. The upper and lower edges of each rectangle coincide with depth contours of the plate interface that are spaced at 1 km (Fig. 1). The rectangles, called subfaults, are

used to compute the coseismic ground deformation (Okada, 1985). Using this discretization of the plate interface, we modeled various tsunami sources by prescribing a general pattern of slip distribution in the proposed rupture, constructed from a combination of slip on the subfaults.

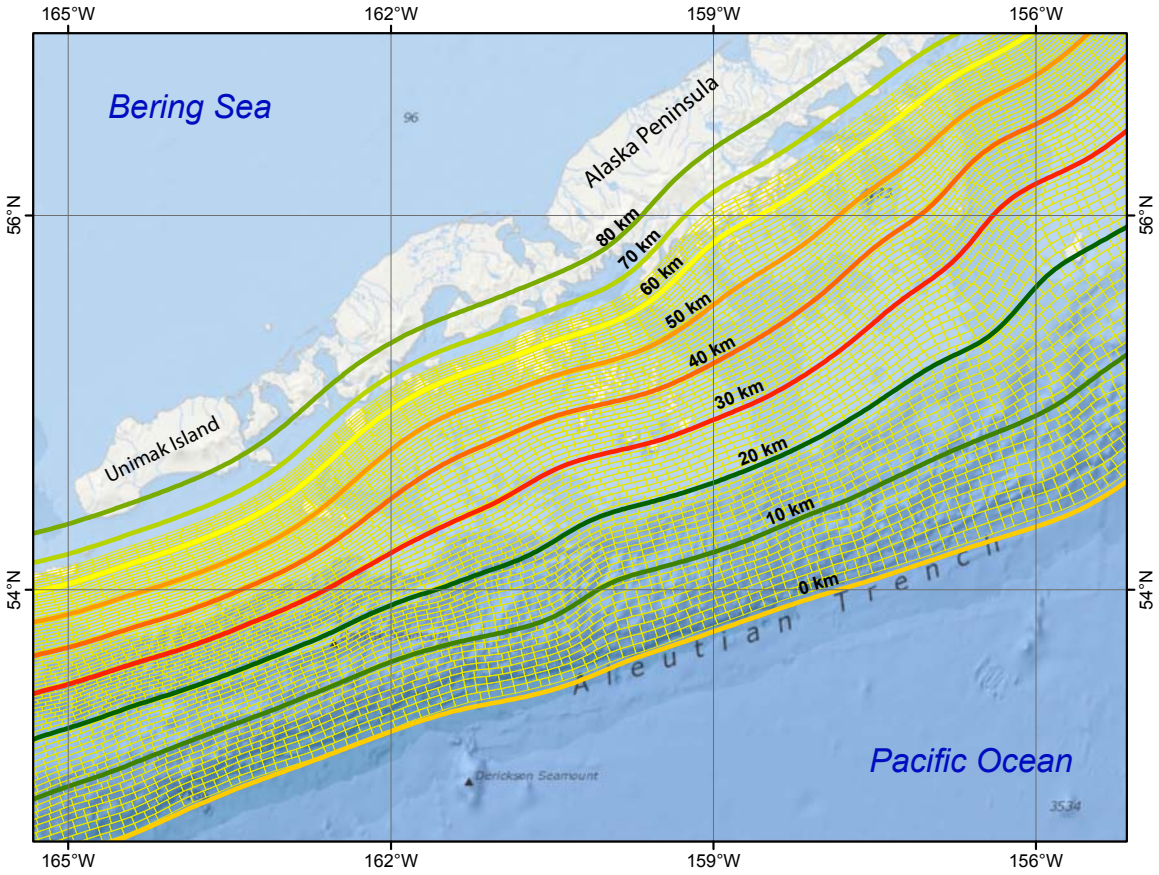

Figure 1. Slab1.0 plate interface model in the western part of the Alaska Peninsula. The small rectangles show our discretization of the interface.

We performed a numerical experiment to determine the sensitivity of the tsunami time series at Unalaska and Sitka to different slip patterns in the 1938 rupture zone. Figure 2 shows the plate interface in the study area, divided into 11 segments in the along-strike direction (i=1:11), and into 27 depth intervals in the down-dip direction (j=1:27). We use this mosaic to develop variable slip distributions within the 1938 rupture. In the downdip direction, we specify three major rupture types: "shallow" (trench to ~30 km depth, intervals 1 to 14), "mid-depth" (~20-40 km depth, intervals 8 to 21), and "deep" (~30-50 km depth, intervals 14 to 27). The shallow rupture corresponds to the inferred locked area based on Fournier and Freymueller (2007), while the mid-depth model approximates the horizontal position of the rupture model of Johnson and Satake (2004). In the along-strike direction, segments 4 through 10 cover the length of the 1938 rupture. Within those segments, we also vary slip along strike, placing the maximum amount of slip either at the western end of the rupture, in the middle of it,

or at its eastern end. Varying the slip along strike in this manner for each of the three depth intervals, we construct a total of 9 sources within the 1938 rupture area. All sources have the same seismic moment, equal to that of the 1938 earthquake. Figure 3 shows the coseismic vertical seafloor displacement for three ruptures that have slip placed at the different depth intervals, and Figure 4 shows the seafloor displacements with variation of slip in the along-strike direction.

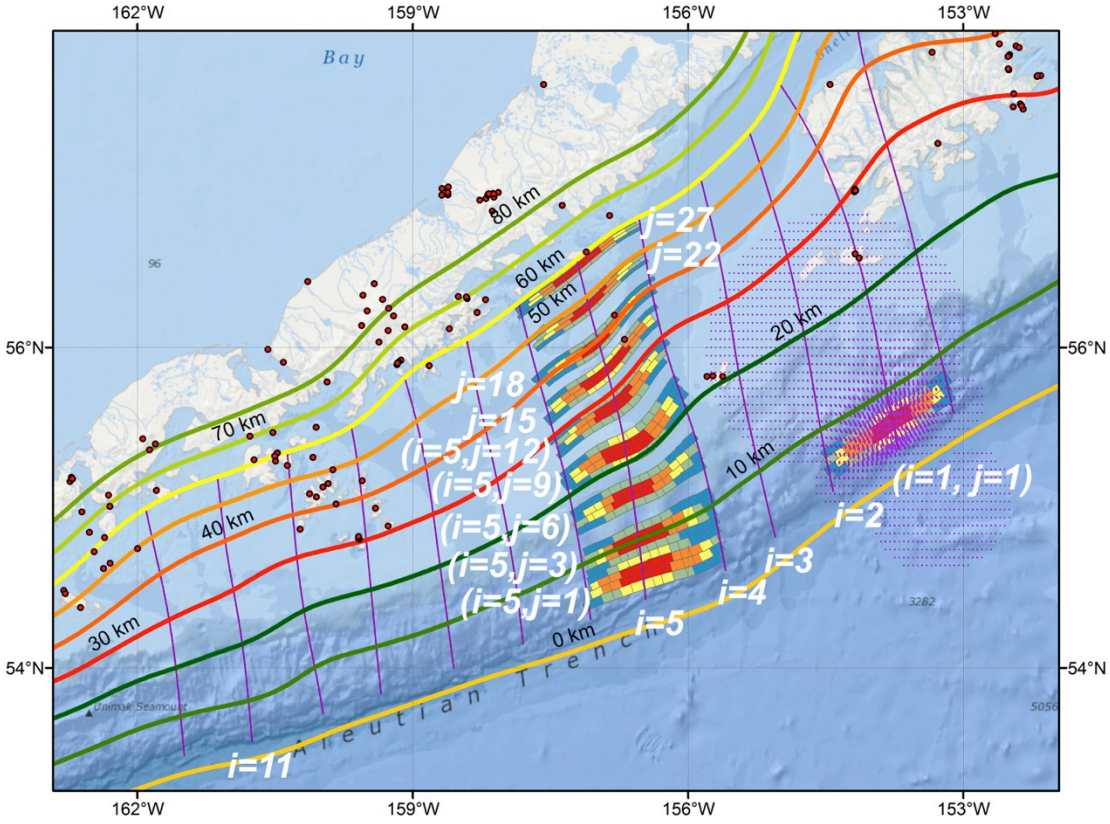

Figure 2. Example slip distributions for the mosaic of sub-events used to construct the slip distribution of larger events. At each grid point (defined by the intersection of a line parallel to depth and a line in the downdip direction, we place a unit slip distribution that is smooth and centered on the grid point. Red colors indicate high slip, and cool colors indicate low slip. Larger slip events can be constructed by scaling and summing these unit sources. Note that only every third source is shown in the downdip direction for clarity.

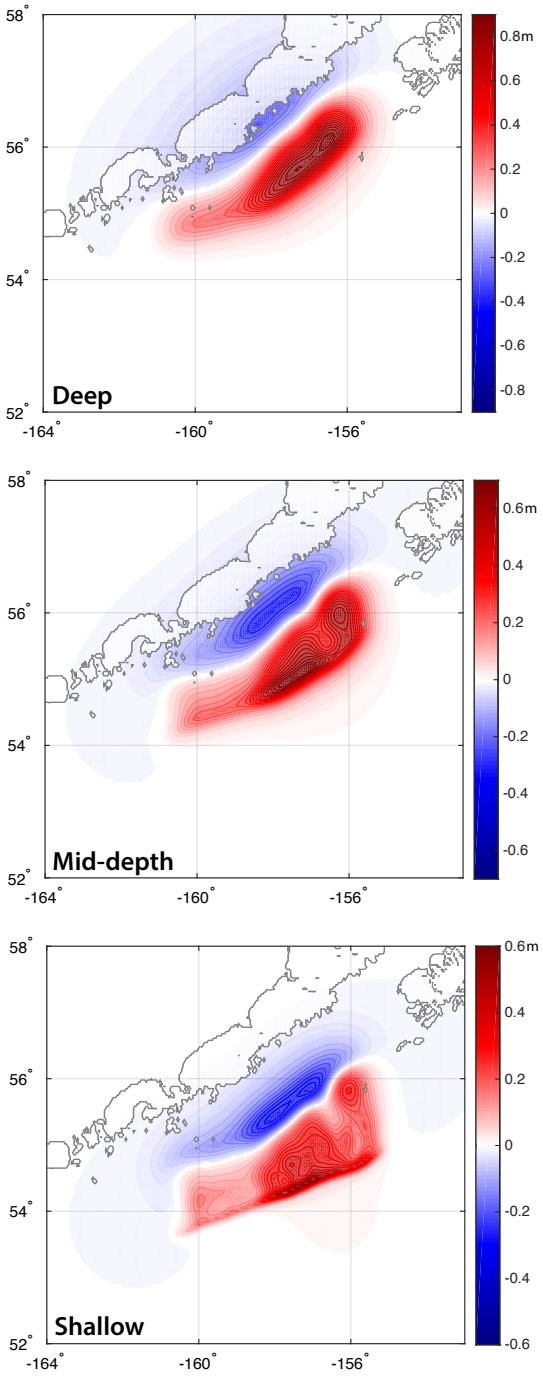

Figure 3. Vertical seafloor displacements caused by the shallow, mid-depth and deep slip distribution scenarios. Displacements are in meters.

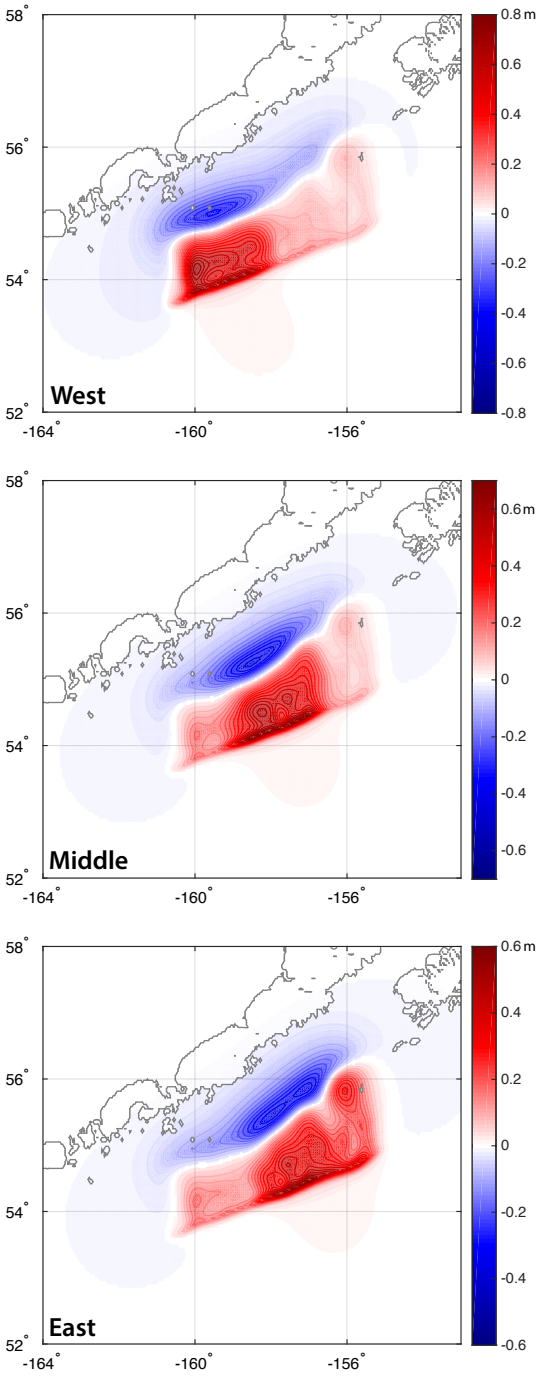

Figure 4. Vertical seafloor displacements caused by the along-strike slip distribution scenarios. Displacements are in meters.

For each modeled slip distribution on the plate interface, we simulated the propagation of the resulting tsunami to Unalaska and Sitka. Figures 5 and 6 show comparisons between the simulated time series for all 9 tsunami sources and the observed tsunami at Unalaska and Sitka, respectively. The results show that the

waveforms corresponding to deep sources disagree with the observations at both locations. Also, ruptures with the major amount of slip placed at the western end of the rupture produce wave amplitudes at Unalaska that are significantly larger than the recorded wave. Since Unalaska is much closer to the source area than Sitka, it is more sensitive to the along-strike variations in the slip distribution. Overall, the mid-depth and shallow sources with the major slip at the eastern part of the rupture fit the observations best. Sitka has essentially no sensitivity to the location of slip, but is sensitive to the depth. Shallow and mid-depth sources fit the data at Sitka well, but the deep source does not.

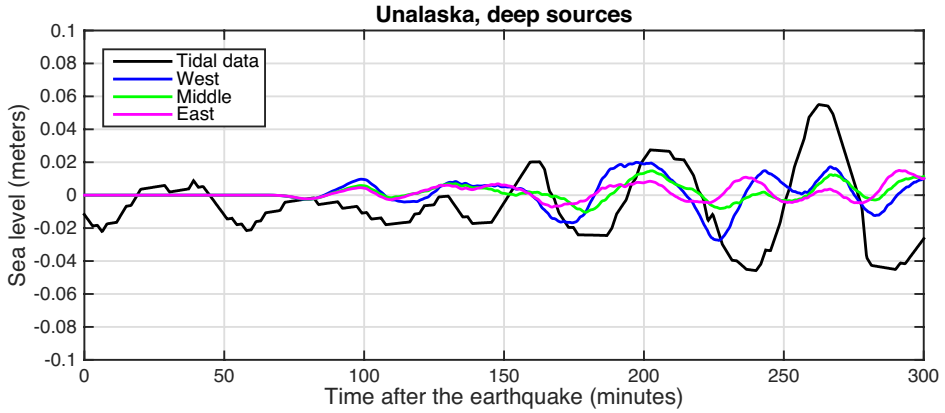

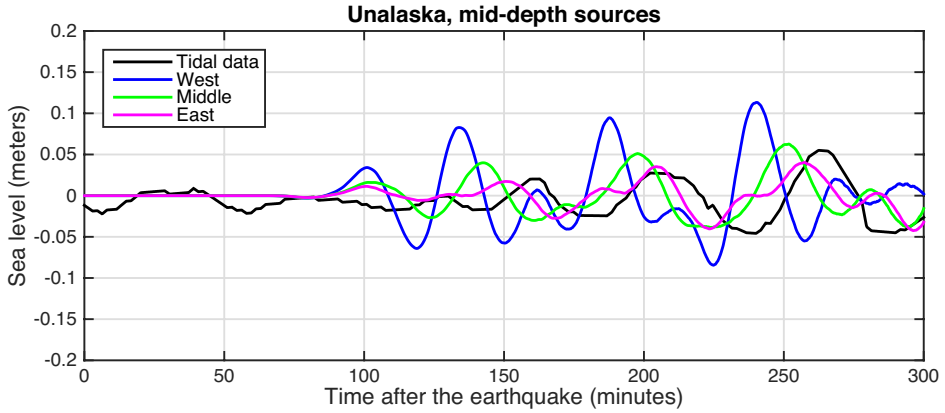

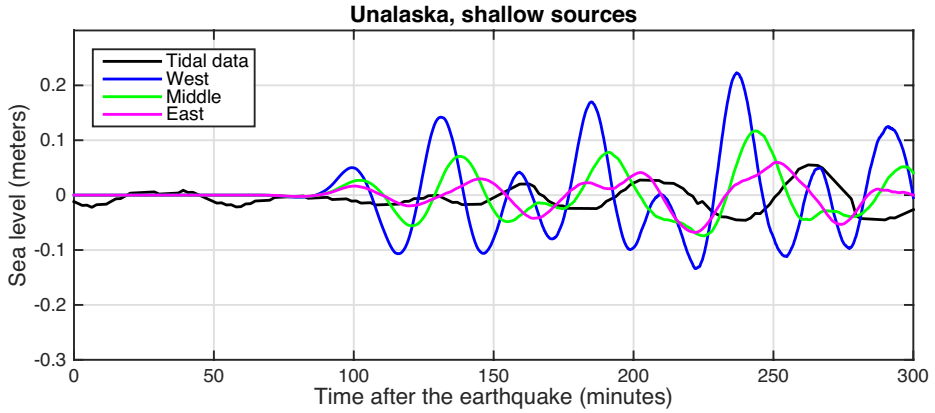

Figure 5. Tide gauge data from the Unalaska tide gauge, and predictions from the full range of models (west, middle, and eastern sources, at three different depth ranges). The Unalaska tide gauge is poorly fit by the western source model, suggesting limited slip in that region in 1938, and is better fit by the mid-depth source models. For a shallow or mid-depth source, the eastern model fits better than the middle or western model.

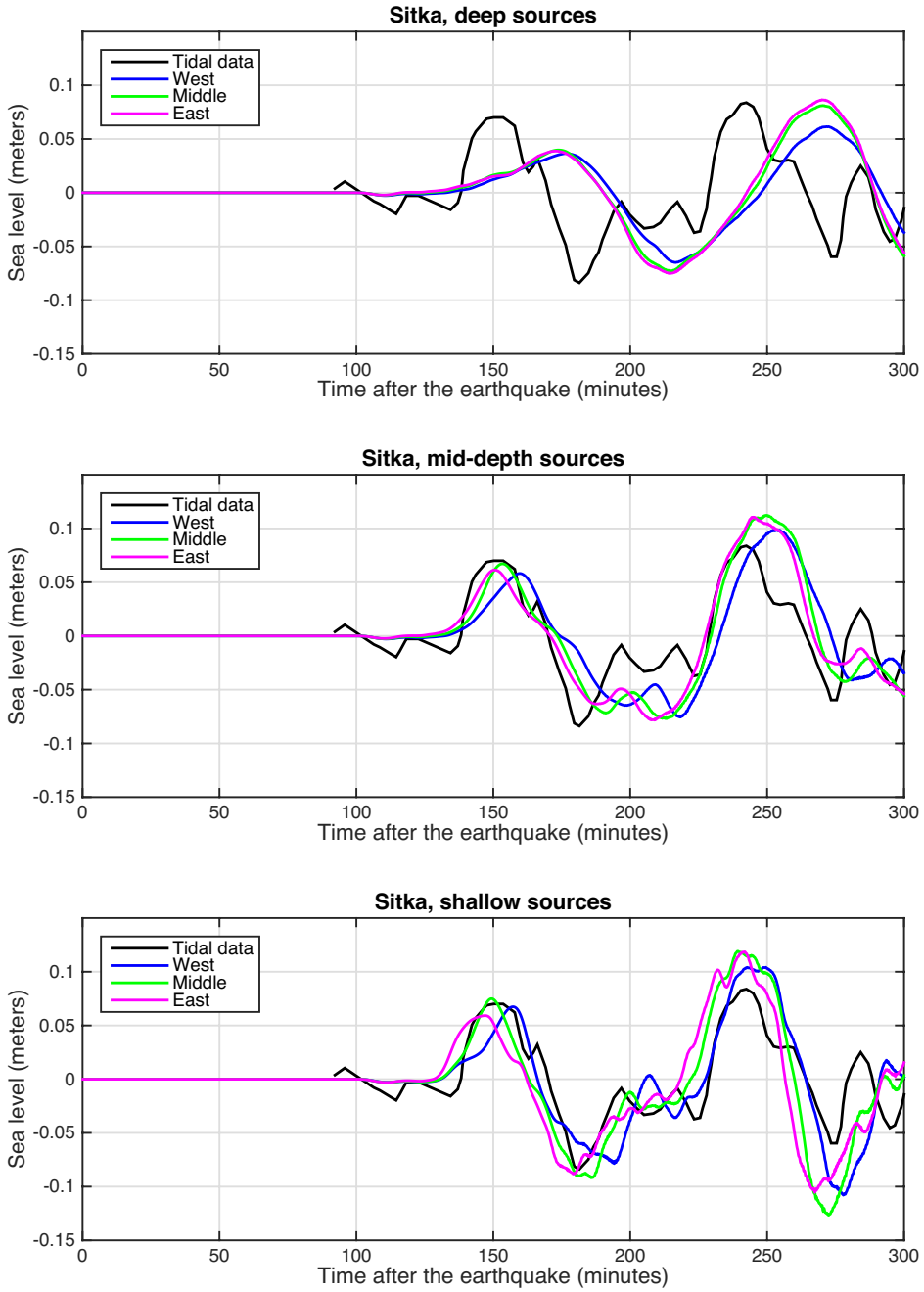

Figure 6. Sitka tide gauge data and predictions from the range of source models, as in Figure 5. The Sitka tide guage is insensitive to the location of slip, and can be fit well by either a shallow or mid-depth source.

To test the easternmost possible extent of the 1938 rupture, we shifted the source along strike to the east, using segments 2 through 8 instead of 4 to 10 (Fig. 2). The resulting coseismic deformation is called “far east” and is shown in Figure 7. We compare the waveforms produced by the “east” and the “far east” shallow sources with observations at Unalaska and Sitka (Figure 7). The simulated

waveforms are very similar at Sitka, both having the fist arrival before the observed wave. The simulated time series at Unalaska differ in amplitude, and it is not clear whether either of them fits the observations better. The eastern source fits the amplitude better, but the far eastern source matches the phase better; only a slight rescaling, well within the uncertainty in the moment, would be required to make the far eastern source match the amplitude as well.

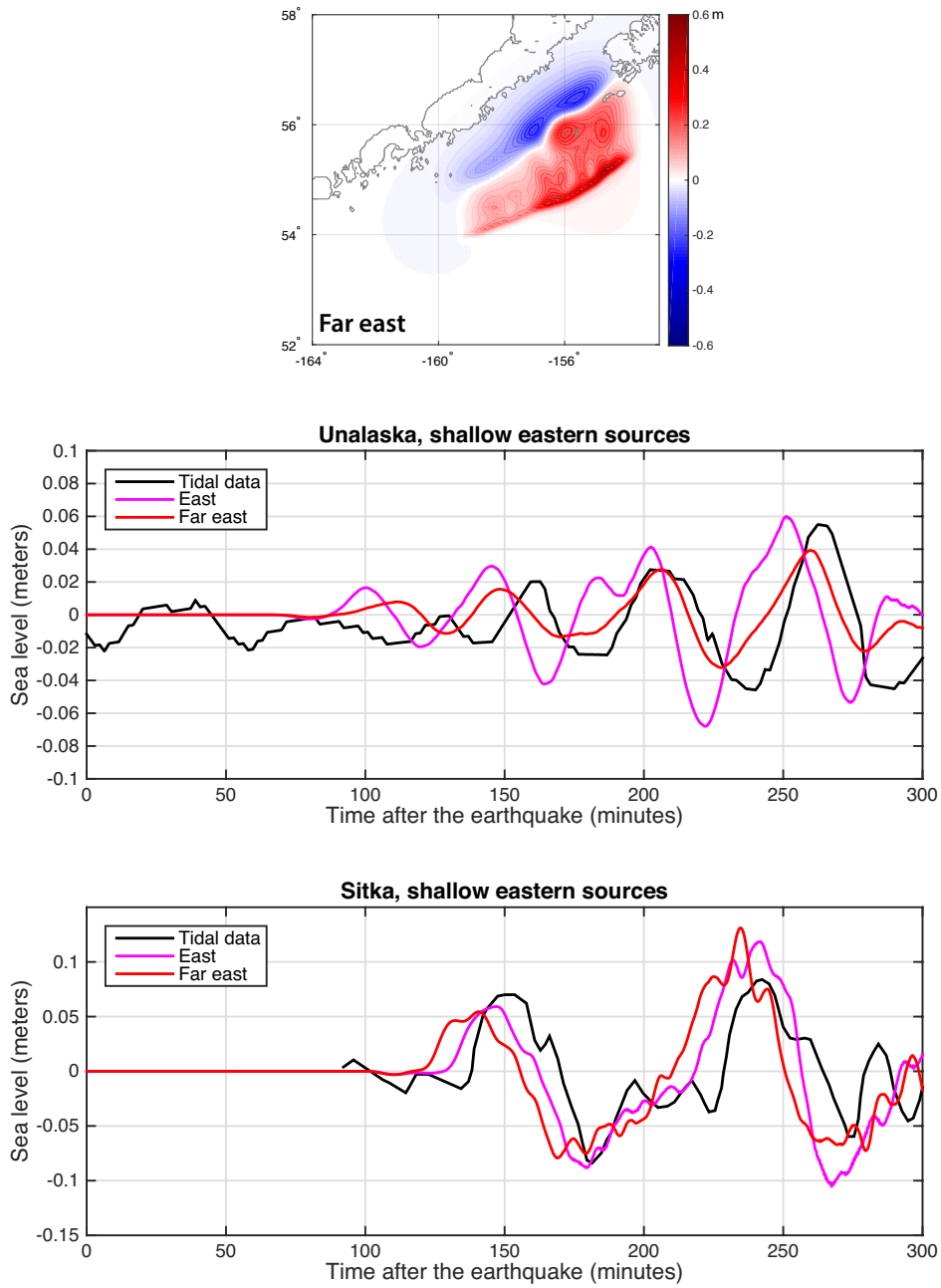

Figure 7. Vertical seafloor displacements (top) and tide gauge data and model predictions for a far eastern source model.

Overall, the tsunami simulations show that either shallow or mid-depth sources can provide a good fit to the data. GPS horizontal data are better fit by a model (Figure 8) that corresponds to the shallow model (Fournier and Freymueller, 2007; Li et al., 2018), but the tsunami data cannot rule out the possibility that the 1938 earthquake included slip on the deeper part of the interface. Intriguingly, Li et al. (2018) noted that the GPS vertical velocities are not consistent with the model that fits the horizontal, because that model fails to predict the rapid subsidence of Chirikof Island. A model such as the mid-depth model would be a better fit to those vertical data, although a worse fit to the GPS horizontal data.

The tsunami record at Unalaska/Dutch Harbor is fit best by models that have all slip located as far to the east as possible. Both the "eastern" and "far eastern" models are satisfactory fits to the data. Comparison of these coseismic models to the interseismic model (Figure 8) is intriguing. The "far eastern" model features coseismic slip that is almost entirely located within the "strongly locked" segment of the model of Li et al. (2018), with little to no slip west of the line marked by "1" in Figure 8a. This model would imply that the actual area of major slip in 1938 was much shorter along-strike than has been assumed previously, based on aftershocks. Even with the "eastern" model, the rupture area would be smaller than previously estimated, which might help explain why previous estimates of average slip in the event were so low.

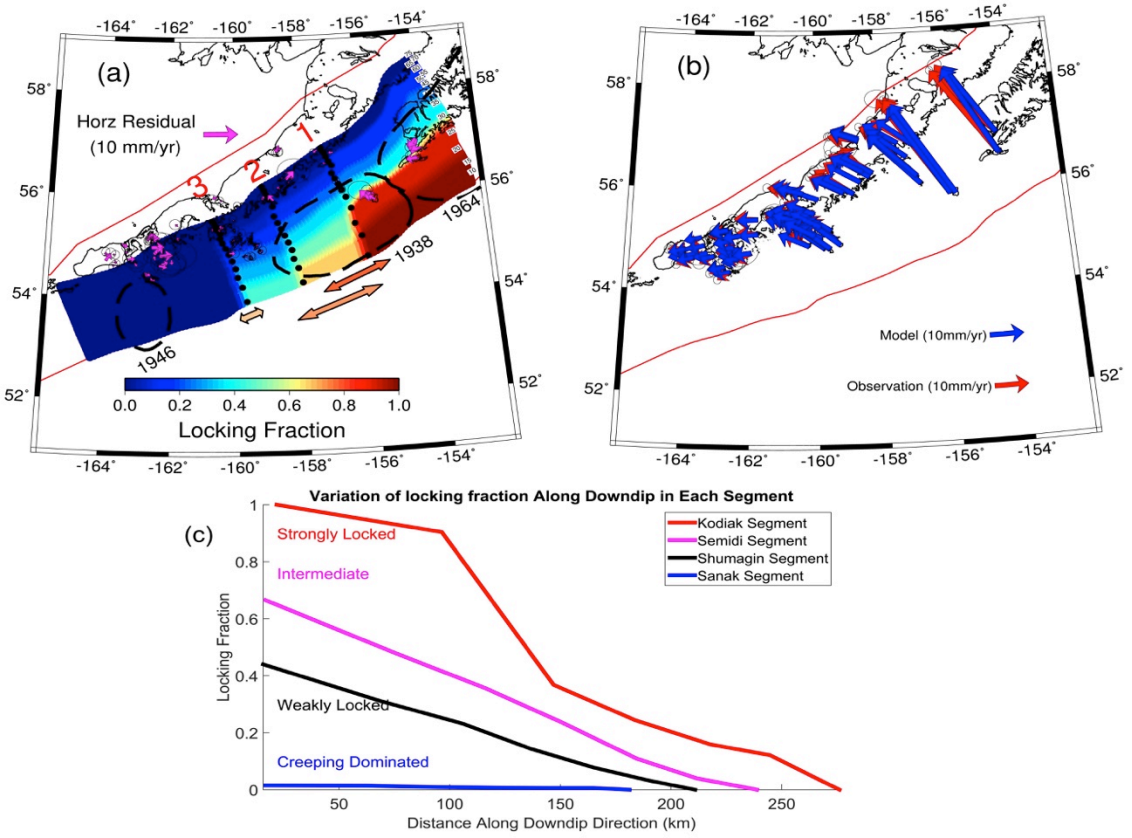

Figure 8. Updated GPS slip deficit model, from Li et al. (2018). (a) Estimated slip deficit model. (b) GPS velocities and model predictions (horizontal only). (c) Profiles of the

slip deficit distribution within each segment of (a). The "far eastern" model of Figure 7 places most slip only within the easternmost segment of this model, labeled "strongly locked".

Both the "eastern" or "far eastern" scenarios are basically consistent with the interseismic slip deficit pattern observed from present-day GPS data. If the "far eastern" model is an accurate depiction of the 1938 coseismic slip, then it is likely that there remains a segment, located just to the east of the Shumagin Islands, which has not ruptured in more than a century, and thus could be ready for rupture at any time. If the "eastern" scenario is more accurate, then it is likely that most of the locked area inferred by GPS ruptured in 1938.

2. Slip distribution of the eastern part of the 1957 rupture

This section is a condensed summary of the published paper by Nicolsky et al. (2016). The 1957 earthquake had an aftershock zone that was ~1200 km long, making it still one of the longest ruptures ever recorded (Figure 9).

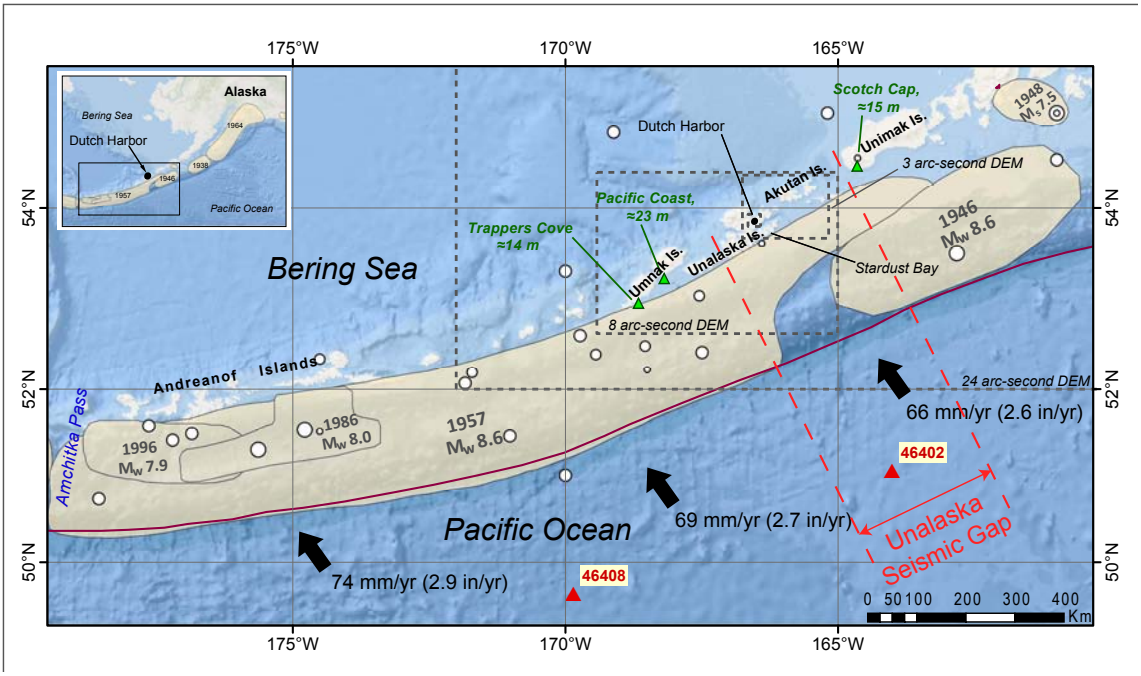

Figure 9. Map showing the central to eastern Aleutians and the presumed rupture areas of the 1957 and 1946 earthquakes.

Historical accounts of tsunami runup in 1957 include 9–23 m high tsunami waves along Pacific-facing Aleutian island shorelines and a far-field tsunami in Hawaii with maximum runups up to 16 m (Lander, 1996; National Geophysical Data Center/World Data Service, NGDC/WDS, 2015). The accounts reported by Lander (1996) include high runups at Chernofski on the northwest coast of Unalaska Island, on the Pacific Ocean side of Umnak Island, and Scotch Cap on Unimak Island. At

Stardust Bay on Sedanka Island (Figure 9), Witter and others (2015) identified drift logs transported by the 1957 tsunami at an elevation of >18 m above mean sea level.

These observations conflict with models of low moment release in the eastern part of the 1957 rupture (House et al., 1981; Johnson et al., 1994). Tsunami models run by Witter et al. (2015) that use the 1957 source model of Johnson et al. (1994) failed to produce tsunami runup that matched observations at Stardust Bay. Alternatively, they used a simple megathrust source model to simulate tsunami inundation and runup that agreed with geological evidence at Stardust Bay. However, they did not compare the simulated tsunami dynamics of their source to the 1957 tide gauge record at Dutch Harbor.

The 1957 tsunami recorded by the tide gauge at Dutch Harbor reached a maximum water level of 0.68 m and produced waves with a period of ~30 minutes. The record was digitized from scanned copies of the marigrams (written communication, Paula Dunbar, NCEI, 2015) of the 1957 tsunami in Dutch Harbor. The tidal and atmospheric components in the tsunami record were filtered using 5 years of hourly water level data (written communication, George Mungov, NCEI, 2015) and a 4-hour running average filter. Comparison of the 1957 tide gauge record obtained from NCEI with the tsunami record published by Lander (fig. 61, 1996) reveals that the tsunami arrives 5 minutes earlier in Lander's copy of the marigram. This discrepancy could be due to digitization errors, a decrease in the rate of tide gauge barrel rotation, or other unknown reasons. Nicolsky et al. (2016) inferred that tsunami models also featured a propagation delay due to bathymetric complexities near the trench and Aleutian arc crust, and concluded that a total time shift of 14 minutes needed to be applied to compare the data with the models.

To reassess the slip distribution in the eastern part of the 1957 aftershock zone, we considered several hypothetical rupture models in the Unalaska seismic gap and compared them with the 1957 observations. Previous analyses placed nearly the entire seismic moment release in 1957 west of 173°W, about 300 km west of Unalaska (House et al., 1981; Johnson et al., 1994). It was recognized that slip occurred east of 173°W, possibly near the western part of Umnak Island and trenchward from Driftwood Bay (Witter and others, 2014), but the slip distribution of Johnson et al. (1994) does not predict tsunami waves that fit the Dutch Harbor tide gauge record well. Particularly important is the prominent strong positive first arriving wave on the Dutch Harbor marigram, where the Johnson et al. (1994) model predicts a slowly increasing first arrival; the amplitude of the first wave is also underpredicted. We infer that the first positive arrival comes from large slip off the Pacific coast of Unalaska Island. We test this hypothesis using a suite of rupture models.

To model Aleutian megathrust ruptures we discretized the 3-D subduction geometry of the Alaska–Aleutian plate interface by Hayes and others (2012) into a number of 3 to 6 km long rectangles (subfaults) along the plate interface, as in our study of the 1938 event. The subfaults' upper and lower edges coincide with depth contours placed every 1 km along the plate interface. Coseismic deformation is

computed for all subfaults using formulas developed by Okada (1985) for an elastic half space.

We considered four hypothetical slip distribution models (A–D), each equivalent to an M_w8.2 earthquake near Unalaska and Akutan Islands. The resulting tsunami predictions can be scaled linearly for larger or smaller amounts of slip. We used theoretical slip distribution formulas by Freund and Barnett (1976) to parameterize and compute coseismic slip on the fault. This allows us to impose a smooth slip distribution using only a few parameters. Figure 10 shows the slip distribution for each model. The scenarios are offset by about 10 km in the downdip direction to test the impact of different rupture depths, such that model A is centered at 40 km depth; model B is centered at 30 km; model C is centered at 20 km; and model D is centered at 10 km. The majority of slip in each model occurs within ±5 km of the central depth. The vertical deformation computed for each model provides the initial input for the tsunami simulation (right column of Figure 10). These scenarios can be combined by superposition, scaling and summing any combination of the scenario models.

The methods we used for simulations of the tsunami propagation and runup are summarized in Nicolsky et al. (2016), and detailed in earlier publications (Nicolsky and others, 2011; Nicolsky, 2012). We assume the initial displacement of the ocean surface is equal to the vertical displacement of the ocean floor during the earthquake rupture process; the contribution of horizontal displacements (Tanioka and Satake, 1996) is not considered. We also assume sea floor displacement is instantaneous; we do not model the finite speed of rupture propagation along the fault. Computations that map tsunami propagation and inundation in detail employ a series of five nested numerical grids with a resolution of 2 arc-minutes; 24, 8, 8/3 arc-seconds; and $\approx 16 \times 16$ meters. The model solves the nonlinear shallow-water equations using a finite-difference method on a staggered grid.

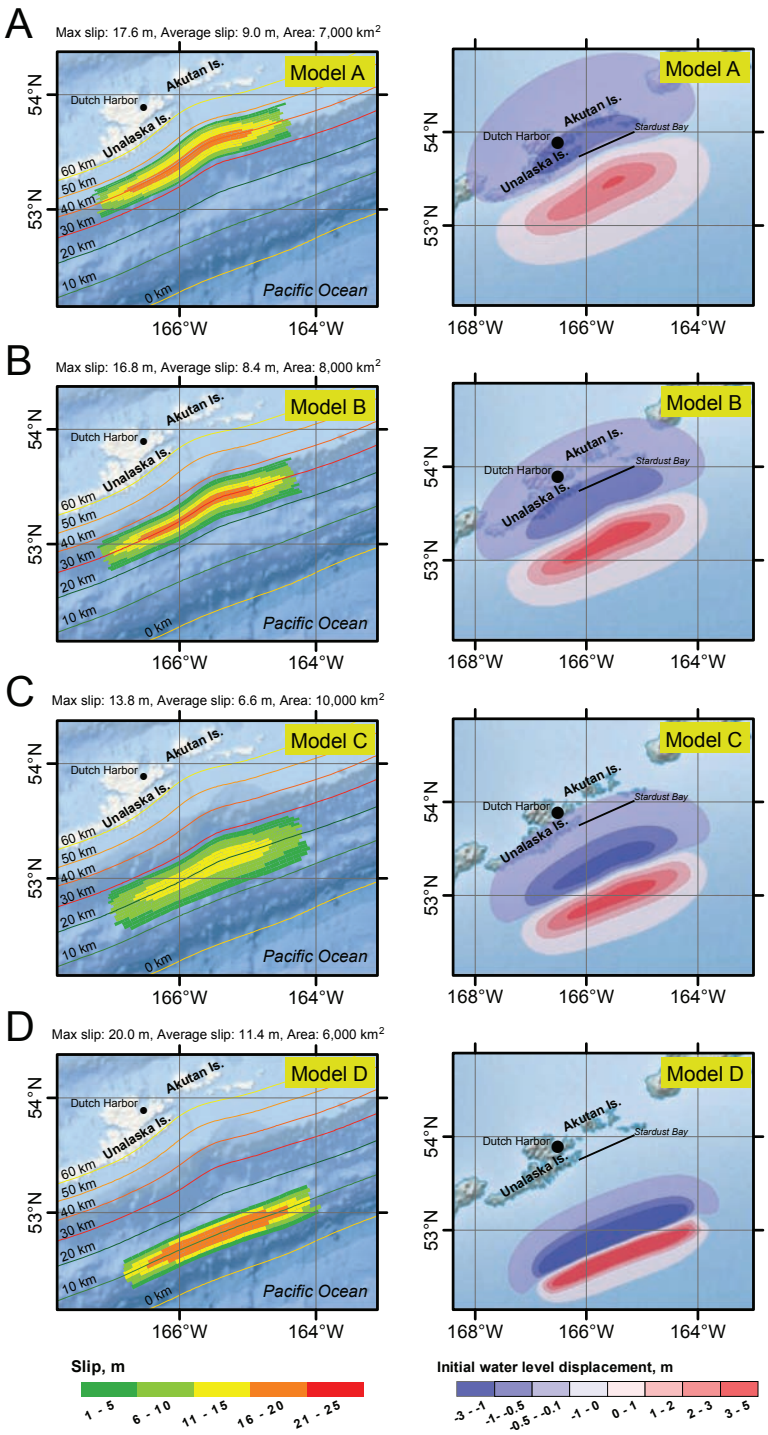

Figure 10. Slip models (left) and vertical seafloor deformation (right) for hypothetical models A-D, which differ in the depth of slip.

Comparison of modeled and observed tsunami records in Dutch Harbor

We compared modeled and observed (de-tided) water level dynamics over several hours after initiation of the 1957 earthquake (Figure 11). Note that 8–50 cm of subsidence in Dutch Harbor occurs in models A-C; the amount of modeled subsidence is indicated in the sub-title of each subplot. The Dutch Harbor tide gauge marigram shows no measurable subsidence in Dutch Harbor during the 1957 earthquake, although Wahr and Wyss (1980) inferred 10-15 cm of subsidence based on annual mean water levels; we concluded that this was most likely a postseismic signal rather than a coseismic signal (Nicolsky et al., 2016). The modeled water level is shown from the perspective of an observer watching a tide gauge that subsides together with the land in Dutch Harbor. In all models, the time between successive waves is ~30 min.

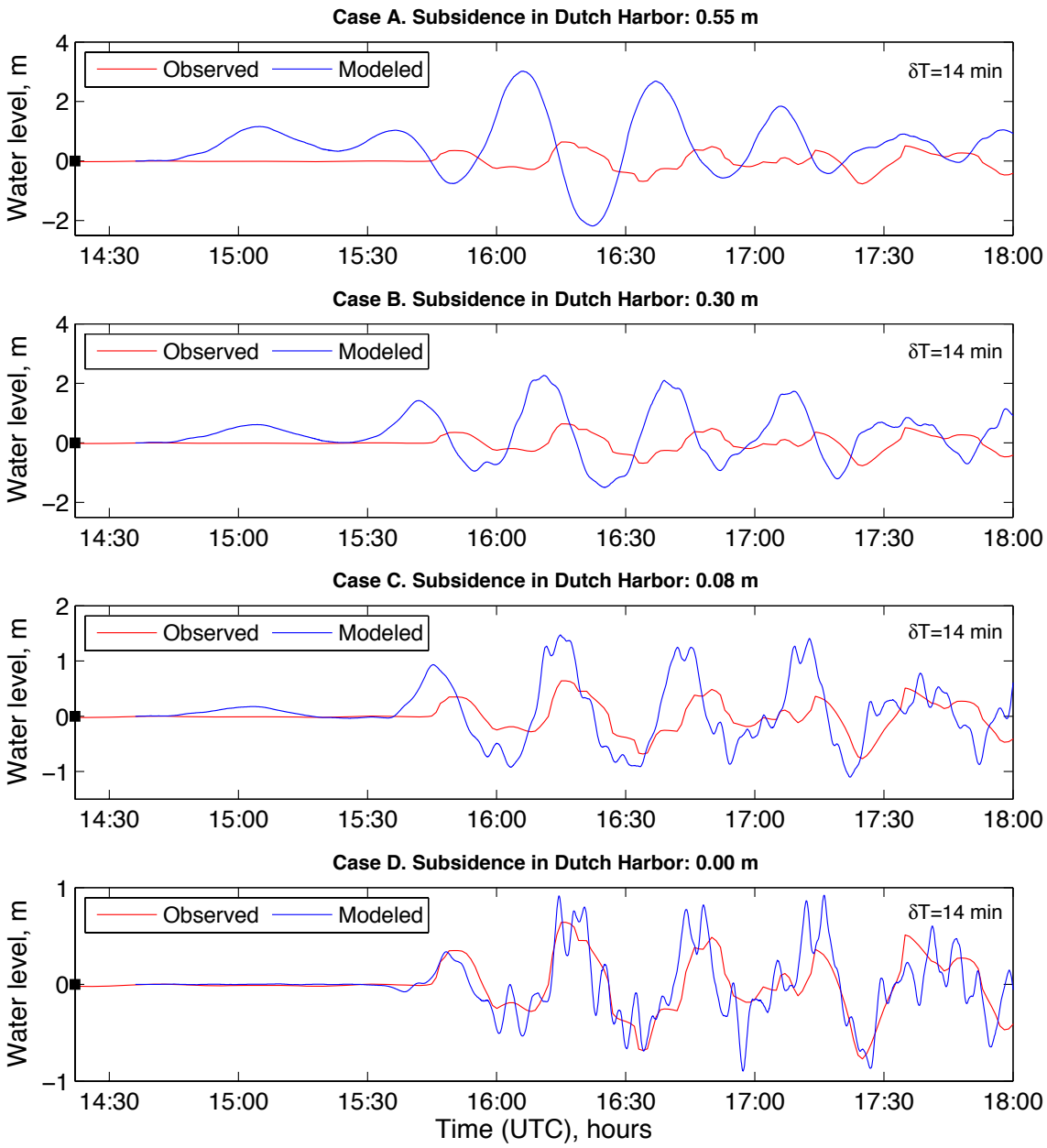

Figure 11. Observed tide gauge record at the Unalaska/Dutch Harbor tide gauge, and tsunami model predictions for scenarios A-D. In addition to the predicted tide gauge record, the panels also show the predicted subsidence at Dutch Harbor. Model D, with the shallowest slip, provides the best match to both the water level and subsidence observations.

The predicted water levels differ considerably in both amplitude and arrival time for the four models. The first wave arrival time is much earlier for models A-C than for model D, and the amplitudes of the waves are larger for the deeper ruptures. This seemingly counter-intuitive result occurs because of the position of the region of coseismic subsidence relative to the islands. The deeper models A and

B produce subsidence on the Bering Sea side of Unalaska Island, and in those models the first arriving waves come from this region, followed soon by waves from the uplifted region. In model C, there is still significant subsidence on the continental shelf and the upper part of the inner trench wall, while in model D the primary tsunami source is located offshore the Pacific side of Unalaska island.

The first wave arrival time changes drastically among the models. The modeling results for models A and B indicate an arrival of the first wave ~20 minutes after the earthquake, which is more than an hour earlier than observed. The first tsunami arrival in model C is also far too early, as a result of the subsidence on the continental shelf, although the main high amplitude arrivals are close to those observed. Based on its amplitude and arrival time, the slip distribution of model D, characterized by shallow near-trench slip, best explains the tide gauge record at Dutch Harbor.

Comparison of modeling results and tsunami runup in Stardust Bay

We also compared the results of the tsunami simulations with geological estimates of tsunami runup in 1957 from Stardust Bay, a funnel-shaped reentrant on the southern coast of Sedanka Island that faces the Aleutian trench. We ran tsunami simulations in Stardust Bay for models A–D and compared the simulated runup produced by each scenario to the elevation of drift logs inferred to have been deposited by the 1957 tsunami (Witter et al., 2015). A line of debris, including drift logs, often delineates the minimum runup after most tsunamis. Witter et al., (2015) found three logs deposited at the elevation of 13-14 m above sea level; they also discovered a higher log containing nails attesting to its historical age. The nailed log was stranded in a narrow gully at an elevation of 18.5 m.

The maximum computed water level varies along the coast of Sedanka Island. The simulated extent of inundation for models B-D agree well with locations of the drift logs at Stardust Bay. The log with nails at 18.5 m lies at the boundary of the simulated inundation limit for model D, and is well within the uncertainty for narrow gullies. The simulations indicate that on the outer coast facing the trench, the maximum runup and inundation is predicted well by any slip model with slip extending along Unalaska Island at depths shallower than 30 km (i.e. models B-D).

A suite of forward models shows that waves generated by a shallow rupture at 5-15 km depth along Unalaska and Akutan Islands can reproduce the observed initial wave arrival at the Dutch Harbor tide gauge during the 1957 earthquake. Waves generated by ruptures deeper than 20-25 km arrive sooner than those observed in 1957. A shallow rupture, such as the one illustrated in model D, with about 20 m of maximum slip can generate a tsunami that explains both the tsunami runup in Stardust Bay and the tide gauge record at Dutch Harbor. Additional numerical experiments show that a shallow 10-km-deep rupture along Unimak and Akutan Islands and rupture scenarios at depths of 20 km along Unalaska and Umnak Islands provide a satisfactory fit to the tide gauge record, but underpredict the

runup at the Stardust Bay (Nicolsky et al., 2016). In addition, shallow rupture along Unimak and Akutan Islands can explain the 12.5–15 m high waves observed at Scotch Cap on Unimak Island in 1957. Although details remain obscure because of sparse tsunami observations, the simulations that are consistent with the Dutch Harbor tide gauge and Stardust Bay geology require substantial shallow slip offshore Unalaska and Akutan Islands in 1957.

Summary

Our results, along with those of Witter and others (2015), suggest a reassessment of the spatial extent of slip in the eastern part of the 1957 aftershock area along Unalaska and Akutan Islands is needed. In the eastern area, aftershocks extend ~500 km beyond the end of significant slip inferred by previous studies (House et al., 1981; Johnson et al., 1994), In contrast, geologic observations at Stardust Bay and the Dutch Harbor tide gauge data are consistent with large slip at shallow depths along the eastern part of the aftershock zone, suggesting that the rupture length is reasonably approximated by the 1200-km long zone of aftershocks. If the 1957 rupture did extend along the entire 1200-km-long aftershock zone, then the current estimates of earthquake magnitude (M_w 8.6) is too low. Indeed, the current estimate makes the 1957 earthquake a notable global outlier from empirical relations between earthquake magnitude and rupture length (Henry and Das, 2001).

Models that limit moment release to the western part of the 1957 aftershock zone, like the model of Johnson et al. (1994), rely on the assumption that P-wave amplitudes recorded at station PER in Perth Australia were decaying before PP arrivals, which requires little slip after the first 4 minutes of the rupture. However, it is possible that large P-waves that arrived later during the bilateral rupture could be hidden within the PP wavetrain; indeed, this possibility was noted by House et al. (1981) who proposed that the coda might have obscured the signal of delayed or slow rupture in 1957.

Geological evidence at Stardust Bay, eye-witness accounts of tsunami heights, and our modeling results imply that the eastern part of 1957 earthquake rupture likely had substantial slip along a section of the megathrust that is poorly coupled today (Freymueller et al., 2008). These observations can be reconciled if slip and slip deficit are mainly confined to the shallow, near-trench region where geodetic observations on the islands have little resolution. A more comprehensive model of the 1957 rupture that considers several possible slip modes offshore Unalaska and Akutan Islands in 1957 might unite the geologic and tide gauge observations with previous studies.

To further resolve the details of moment release during the 1957 earthquake, modeling should incorporate local geological and tide gauge observations of tsunami wave dynamics as well as far-field tsunami waveforms recorded around the Pacific Ocean. With improved constraints from tsunami observations, new models of the 1957 rupture should evaluate multiple possible rupture modes along strike,

including dynamic rupture in poorly coupled areas, and delayed, shallow slip that may be evident in the long-duration seismic waveforms produced by great earthquakes.

Publications Resulting from this Work

Li, S., and J. T. Freymueller (2018), Spatial Variation of slip behavior beneath the Alaska Peninsula along Alaska-Aleutian Subduction Zone, *Geophysical Research Letters*, 2017GL076761.

Nicolsky, D. J., J. T. Freymueller, R. C. Witter, E. N. Suleimani, and R. D. Koehler (2016), Evidence for shallow megathrust slip across the Unalaska seismic gap during the great 1957 Andreanof Islands earthquake, eastern Aleutian Islands, Alaska, Geophys. Res. Lett., 43, 10,328–10,337, doi:10.1002/2016GL070704.

References

Boyd, T.M., and Jacob, K., 1986, Seismicity of the Unalaska region, Alaska: Bulletin of the Seismological Society of America, v. 76, no. 2, p. 463–481.

Fletcher, H. J., J. Beavan, J. Freymueller, and L. Gilbert, High interseismic coupling of the Alaska subduction zone SW of Kodiak island inferred from GPS data, *Geophys. Res. Lett.*, 28, 443-446, 2001.

Fournier, T. J., and J. T. Freymueller (2007), Transition from locked to creeping subduction in the Shumagin region, Alaska, Geophys. Res. Lett., 34, L06303, doi:10.1029/2006GL029073

Freund, L.B., and Barnett, D.M., 1976, A two-dimensional analysis of surface deformation due to dip-slip faulting: Bulletin of the Seismological Society of America, v. 66, p. 667–675.

Freymueller, J. T., GPS – Tectonic Geodesy, in Encyclopedia of Solid Earth Geophysics, H. Gupta, ed., Springer-Verlag, 2011.

Freymueller, J.T., H. Woodard, S. Cohen, R. Cross, J. Elliott, C. Larsen, S. Hreinsdottir, C. Zweck (2008), Active deformation processes in Alaska, based on 15 years of GPS measurements, in *Active Tectonics and Seismic Potential of Alaska,* AGU Geophysical Monograph, 179, J.T. Freymueller, P.J. Haeussler, R. Wesson, and G. Ekstrom, eds., pp. 1-42, AGU, Washington, D.C.

Hayes, G.P., Wald, D.J., and Johnson, R.L., 2012, Slab1.0—A three-dimensional model of global subduction zone geometries: Journal of Geophysical Research, v. 117, no. B1, 1 p. doi:10.1029/2011JB008524

Henry, C., and S. Das (2001), Aftershock zones of large shallow earthquakes: fault dimensions, aftershock area expansion and scaling relations, *Geophysical Journal International*, *147*(2), 272-293.

House, L.S., Sykes, L.R., Davies, J.N., and Jacob, K.H., 1981, Identification of a possible seismic gap near Unalaska Island, eastern Aleutians, Alaska, *in* Simpson, D.W., and Richards, P.G.,eds., Earthquake Prediction—An International Review: American Geophysical Union, Maurice Ewing Series, no. 4, p. 81–92.

Johnson, J. M., and K. Satake (1994), Rupture extent of the 1938 Alaskan earthquake as inferred from tsunami waveforms, Geophys. Res. Lett., 21, 733-736.

Johnson, J.M., Tanioka, Yuichiro, Ruff, L.J., Satake, Kenji, Kanamori, Hiroo, and Sykes, L.R., 1994, The 1957 Great Aleutian Earthquake: Pure and Applied Geophysics, v. 142, no. 1, p. 3–28.

Lander, J.F., 1996, Tsunamis affecting Alaska, 1737–1996: Boulder, CO, National Oceanic and Atmospheric Administration, National Geophysical Data Center (NGDC), Key to Geophysical Research Documentation, v. 31, 155 p.

Lay, T., and Bilek, S., 2007. Anomalous earthquake ruptures at shallow depths on subduction zone megathrusts. The Seismogenic Zone of Subduction Thrust Faults, Chapter 15, in Dixon, T.H. and Moore, J.C. (eds), Columbia Univessity Press, pp. 476–511.

Li, S., and J. T. Freymueller (2018), Spatial Variation of slip behavior beneath the Alaska Peninsula along Alaska-Aleutian Subduction Zone, *Geophysical Research Letters*, 2017GL076761.

National Centers for Environmental Information/World Data Service (NCEI/WDS), in progress, Global historical tsunami database at NGDC, 2100 BC to present (interactive map): National Geophysical Data Center, NOAA. doi:10.7289/V5PN93H7

Nicolsky, D.J., Suleimani, E.N., and Hansen, R.A., 2011, Validation and verification of a numerical model for tsunami propagation and runup: Pure and Applied Geophysics, v. 168, p. 1,199–1,222. doi:10.1007/s00024-010-0231-9

Nicolsky, D.J., 2012, Alaska tsunami model, *in* Proceedings and Results of the 2011 NTHMP Model Benchmarking Workshop: Boulder, CO, U.S. Department of Commerce/NOAA/NTHMP, NOAA Special Report, p. 55–87, http://nthmp.tsunami.gov

Nicolsky, D. J., J. T. Freymueller, R. C. Witter, E. N. Suleimani, and R. D. Koehler (2016), Evidence for shallow megathrust slip across the Unalaska seismic gap during the great 1957 Andreanof Islands earthquake, eastern Aleutian Islands, Alaska, Geophys. Res. Lett., 43, 10,328–10,337, doi:10.1002/2016GL070704.

Okada, Yoshimitsu, 1985, Surface deformation due to shear and tensile faults in a half-space: Bulletin of the Seismological Society of America, v. 75, no. 4, p. 1,135–1,154.

Savage, J. (1983), A dislocation model of strain accumulation and release at a subduction zone, J. Geophys. Res., 88, 4984–4996.

Tanioka, Y., Satake, K., 1996. Tsunami generation by horizontal displacement of ocean bottom. Geophysical Research Letters 23 (8), 861–864.

Witter, R. C., G. A. Carver, R. W. Briggs, G. Gelfenbaum, R. D. Koehler, S. La Selle, A. M. Bender, S. E. Engelhart, E. Hemphill-Haley, *and* T. D. Hill *(*2015*),* Unusually large tsunamis frequent a currently creeping part of the Aleutian megathrust, Geophys. Res. Lett., 42, *doi:*10.1002/2015GL066083.